Spacer Asn Determines the Fate of Kunitz (STI) Inhibitors, as Revealed by Structural and Biochemical Studies on WCI Mutants‡

Jhimli Dasgupta, Susmita Khamrui, Jiban K. Dattagupta, and Udayaditya Sen*

Crystallography and Molecular Biology Division, Saha Institute of Nuclear Physics, 1/AF Bidhan Nagar, Kolkata 700 064, India

Received February 23, 2006; Revised Manuscript Received April 12, 2006

ABSTRACT: The scaffold of serine protease inhibitors plays a significant role in the process of religation which resists proteolysis of the inhibitor in comparison to a substrate. Although the role of the conserved scaffolding Asn residue was previously implicated in the maintenance of the binding loop conformation of Kunitz (STI) inhibitors, its possible involvement in the prevention of proteolysis is still unexplored. In this paper, we have investigated the specific role of the spacer Asn in the prevention of proteolysis through structural and biochemical studies on the mutants where Asn14 of winged bean chymotrypsin inhibitor (WCI) has been replaced by Gly, Ala, Thr, Leu, and Gln. A residue having no side chain or β-branching at the 14th position creates deformation and insufficient protrusion of the binding loop, and as a result N14G and N14T lose the ability to recognize proteases. Although the reactive site loop conformation of N14A and N14Q are almost identical to WCI, biochemical results present N14A as a substrate indicating that the methyl group of Ala14 is not suitable to capture the cleaved parts together for religation. The poor inhibitory power of N14L points toward the chemical incompatibility of Leu at the 14th position, although its size is the same as Asn; on the other hand, slight loss of inhibitory potency of N14Q is attributed to the inappropriate placement of the Gln14 polar head, caused by the strained accommodation of its bigger side chain. These observations collectively allow us to conclude that the side chain of spacer Asn fits snugly into the concave space of the reactive site loop cavity and its ND2 atom forms hydrogen bonds with the P2 and P1′ carbonyl O at either side of the scissile bond holding the cleaved products together for religation. Through database analysis, we have identified such spacer asparagines in five other families of serine protease inhibitors with a similar disposition of their ND2 atoms, which supports our proposition.

The protein inhibitors of serine proteases inhibit their cognate enzymes by binding tightly at the active site of the enzyme in a substrate-like manner (*1*, *2*), and they undergo cleavage extremely slowly (*3*) compared to a good substrate. The consensus model of serine protease−substrate/inhibitor reaction consists of the chemical steps given in eq 1:

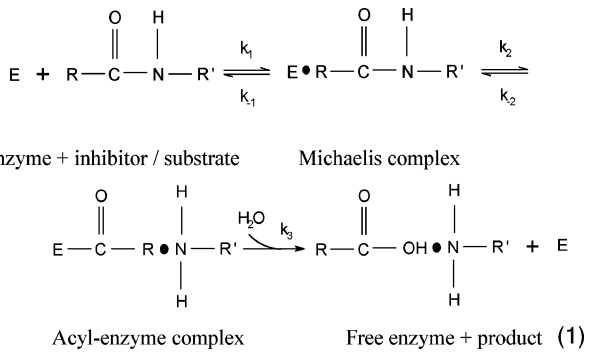

(1)

The enzyme is represented by E and the N- and C-terminal fragments, produced after the cleavage of the scissile peptide bond of the inhibitor, are denoted by R and R′, respectively (*3*).

The canonical serine protease inhibitors comprise of at least 18 convergently evolved families (*4*) that display a strikingly similar backbone conformation around the scissile peptide bond (*2*, *3*), although the scaffold of these inhibitors differ widely in their folds. The interaction between the binding loop and its scaffold is distinctly different in each inhibitor family (*2*), and the assessment of the relative contributions of these interactions toward the binding loop conformation and inhibitory function is of importance to understand and improve the efficacy of the inhibitors. The binding loop conformation in most canonical inhibitors is maintained by one or two disulfide bridges connecting the loop residue(s) with the hydrophobic core (*4*). In others, this loop conformation is maintained by an elaborate network of hydrogen bonds through the side chain(s) of the residues extending from scaffold (*5*, *6*) or by a combination of both. Thus, it appears that the structure and function of serine protease inhibitors can be modulated by the alteration of the scaffolding residues. In chymotrypsin inhibitor-2 (CI2)[1] of the potato inhibitor-1 (PI-1) family, Arg65 and Arg67 extend in a parallel fashion from the protein scaffold to form hydrogen bonds with the binding loop (*3*) and act as a spacer. Radisky et al. showed that mutations of these arginines and

‡ The PDB codes for N14G, N14A, N14T, and N14Q are 2BEA, 2ET2, 2BEB, and 2ESU, respectively.

* To whom correspondence should be addressed. Tel: 91-33-2337-0379. Fax: 91-33-2337 4637. E-mail: udayaditya.sen@saha.ac.in.

10.1021/bi060374q CCC: $33.50
Published on Web 05/17/2006

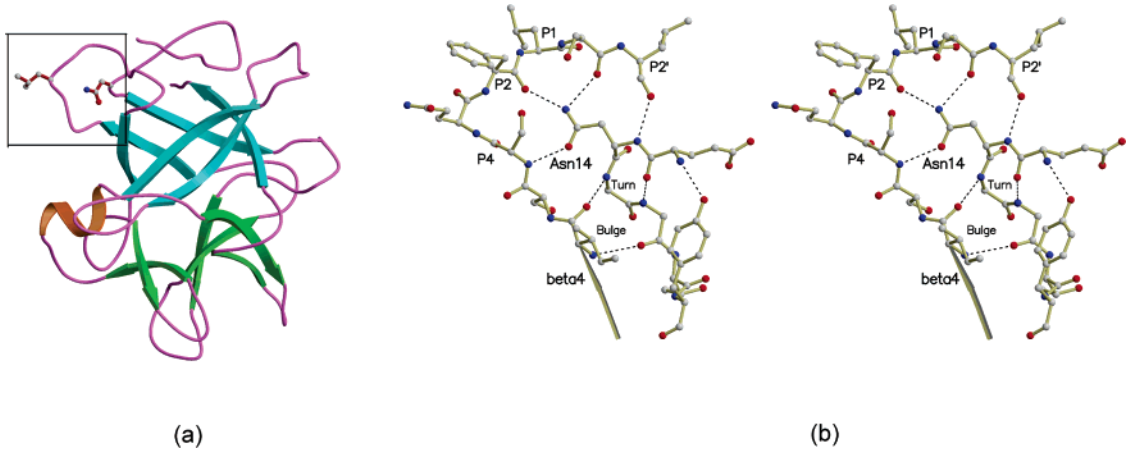

FIGURE 1: (a) Three-dimensional structure of winged bean chymotrypsin inhibitor, WCI, a β-trefoil protein belonging to the Kunitz (STI) family and (b) stereoscopic representation of the hydrogen-bonding interactions made by the scaffolding residue Asn14 with the reactive site loop residues in WCI.

a few loop residues that interact with Arg65 and Arg67 render the binding loop less resistant toward proteolysis, and from this study they proposed a role for these parallel spacer arginines as well as for other scaffolding residues in keeping the leaving group in place that prevents hydrolysis and favors religation (*7*−*9*). However, they correctly pointed out that the pervasiveness of their proposed mechanism needs to be experimentally explored with enzymes and inhibitors beyond subtilisin BPN′ and CI2 (*9*). It is also noted that out of 18 serine protease inhibitor families, parallel spacer arginines are present only in the PI-1 family. Hence, to propose a more generalized mechanism of inhibition for serine protease inhibitors, it is desirable to extend this investigation to other families of inhibitors. For this purpose, scaffolding residue(s) of an inhibitor whose scaffold−binding loop interactions are common to a larger number of inhibitor families should be targeted.

The inhibitors of the Kunitz (STI) family have a characteristic β-trefoil fold, and they mostly inhibit chymotrypsin clan enzymes. Structural studies on Kunitz (STI) inhibitors revealed that a conserved scaffolding Asn residue, through a network of hydrogen bonds (as shown in case of WCI in Figure 1), maintains the conformation of the reactive site loop, which is necessary for proper enzyme recognition (*10*−*12*). However, the detailed role that this conserved Asn plays in the inhibitory mechanism has yet to be explored properly. Interestingly, our structural database investigation (using coordinates from PDB) identified a similar spacer Asn in five other families of serine protease inhibitors, and these asparagines are highly conserved in their respective families. We have chosen winged bean chymotrypsin inhibitor (WCI) of the Kunitz (STI) family to investigate the role of spacer Asn through mutagenesis studies. Our previous mutagenesis studies showed that the replacement of Asn14 by Asp and Lys has no effect on the reactive site loop conformation and on the inhibitory property of WCI (*13*). The molecular dynamics simulations and docking studies that we performed on in silico mutants of WCI predicted the conformational variability and possible range of movement of the reactive site loop caused by the mutations at Asn14 (*14*). However, this study could not shed light on the important events occurring after acyl enzyme formation (eq 1). Hence, to decipher the role of spacer Asn14 in the inhibitory mechanism, we have now performed structural and functional studies on the mutants where Asn14 of WCI is replaced by judiciously chosen amino acid residues such as Gly, Ala, Thr, Leu, and Gln. Crystal structures of four mutants (N14G, N14A, N14T, and N14Q) and biochemical data measured in the presence of chymotrypsin for all the five mutants compared against each other as well as against the native protein WCI revealed the definite spatial and chemical role played by the spacer Asn in the inhibitory mechanism of the Kunitz (STI) family. This proposed role of Asn is further supported and extended by a structural database analysis that we performed with five other families of serine protease inhibitors possessing the conserved spacer Asn.

EXPERIMENTAL PROCEDURES

Site Directed Mutagenesis, Expression, and Purification. The mutation primers were designed (MWG-Biotech and Neuprocell) to replace the scaffolding residue Asn14 by Gly, Ala, Thr, Leu, and Gln. Mutagenesis experiments were performed following the protocols described before (*15*). The sequences of the primers are given below (restriction sites are underlined and mutation sites are given in bold); CI-Nde1: 5′-TGG ACT G<u>CA TAT G</u>GA TGA TGA TTT GGT CGA T-3′; CI-BamH1: 5′-GTA <u>GGA TCC</u> GGA TGA GAA GTG CTT AAT-3′; N14G-F: 5′-AAC TTA GTT GAA **GGT** GGT GGC ACA TAC-3′; N14G-R: 5′-GTA TGT GCC ACC **ACC** TTC AAC TAA GTT-3′; N14A-F: 5′-AAC TTA GTT GAA **GCC** GGT GGC ACA TAC-3′; N14A-R: 5′-GTA TGT GCC ACC **GGC** TTC AAC TAA GTT-3′; N14T-F: 5′-AAC TTA GTT GAA **ACC** GGT GGC ACA TAC-3′; N14T-R: 5′-GTA TGT GCC ACC **GGT** TTC AAC TAA GTT-3′; N14L-F: 5′-AAC TTA GTT GAG **CTC** GGT GGC ACA TAC-3′; N14L-R: 5′-GTA TGT GCC ACC **GAG** CTC AAC TAA GTT-3′; N14Q-F: 5′-AAC TTA GTT GAG **CAG** GGT GGC ACA TAC-3′; N14Q-R: 5′-GTA TGT GCC ACC **CTG** CTC AAC TAA GTT-3′.

The clones were confirmed through sequencing and subcloned in pET28a+ (Novagen) for overexpression. The

[1] Abbreviations: WCI, winged bean chymotrypsin inhibitor; CI2, chymotrypsin inhibitor-2; STI, soybean trypsin inhibitor; ETI, *Erythrina caffra* trypsin/tPA inhibitor; BPTI, bovine pancreatic trypsin inhibitor; MCTI, momordica charantia trypsin inhibitor; PSTI, pancreatic secretory trypsin inhibitor; PI-1, potato inhibitor-1; PDB, Protein Data Bank.

Table 1: Data Collection and Refinement Statistics

	N14G	N14A	N14T	N14Q
Data Collection Statistics				
space group	*P*1	$P6_122$	$P2_12_12$	$P6_122$
cell dimensions (Å, °)	$a = 34.2$; $b = 41.4$; $c = 58.4$; $\alpha = 80.8$; $\beta = 82.4$; $\gamma = 86.4$	$a = b = 60.4$; $c = 212.2$;	$a = 81.5$; $b = 129.5$; $c = 36.5$	$a = b = 60.8$; $c = 213.1$;
molecule(s)/ASU	2	1	2	1
Mathews coefficient, V_m (Å^3/Da)	1.8	2.6	2.2	2.6
completeness (%)	88.4 (80.0)[a]	98.7 (93.7)	94.4 (94.7)	99.3 (95.1)
R_{merge} (%)	4.4 (18)	4.66 (23.6)	12.7 (45)	4.3 (20.8)
resolution (Å)	20−2.35	20−2.1	20−2.8	20−1.94
mosaicity	1.0	0.2	0.6	0.22
average redundancies	1.7	6.96	2.8	6.4
average I/σ	13 (3)	6.9 (2.2)	8 (2)	7 (2.2)
crystal to detector distance (mm)	170	175	175	175
oscillation (°)	1.5	1	1	0.5
Refinement Statistics				
R_{cryst} (%)[b]	21.1	21.3	20.1	21.9
R_{free} (%)[b]	26.3	25.2	25.4	23.8
rmsd[c] bond (Å)	0.007	0.006	0.007	0.005
rmsd bond (°)	1.8	1.7	1.8	1.5
Ramachandran plot (%)[d]				
most favored (%)	83.3	87.8	81.2	89.7
allowed (%)	16.7	12.2	18.8	10.3
disallowed (%)	0	0	0	0

[a] Values in parentheses correspond to the outermost resolution shell. [b] $R_{cryst} = \Sigma_{hkl}||F_o| - |F_c||/\Sigma_{hkl}|F_o|$, 5% of the reflections were excluded for the R_{free} calculation. [c] rmsd, root-mean-square-deviation. [d] Analyzed by PROCHECK.

mutant proteins were expressed in *Escherichia coli* BL21 (DE3) cells as fusion protein, having a 6×His-tag at the N-terminus followed by a thrombin cleavage site, in the presence of kanamycin. In each case, the His-tagged protein was purified from the cell lysate by Ni−NTA (Novagen) affinity column. The 6×His-tag was cleaved by thrombin, and the protein was further purified by gel filtration, using Sephcryl S-100 (Amersham Biosciences) column (78 × 1.4 cm), preequilibrated with a buffer, containing 50 mM Tris (pH 8.0), 100 mM NaCl, and 0.02% NaN_3 at 4 °C. The homogeneity of the purified proteins was checked by 12% SDS−PAGE.

Crystallization and Data Collection. The mutant proteins were concentrated to 10−16 mg/mL in a buffer containing 50 mM Tris (pH 8.0) and 100 mM NaCl. Crystal growth was accomplished using the hanging drop vapor diffusion method against 700 μL of reservoir and incubated at either 4 or 20 °C. N14T crystallizes in a precipitant containing 5% PEG 4 K against 40% PEG 4 K as reservoir, whereas crystals of N14G grew in a mixture of 5% PEG 4 K and 7.5% PEG 2 K as precipitant against 30% PEG 4 K as reservoir. Both N14A and N14Q crystals were grown using Hampton Research Crystal Screen Cryo #15, which contains 25.5% PEG 8 K, 15% glycerol, and 0.17 M ammonium sulfate in 0.085 M Na cacodylate buffer at pH 6.5. Diffraction data for N14G, N14A, N14T, and N14Q were collected up to 2.35, 2.1, 2.8, and 1.94 Å resolutions, respectively, using a 30-cm MAR research image-plate detector with copper Kα radiation from a Rigaku RU-200B rotating anode generator equipped with Osmic MaxFlux confocal optics running at 50 kV and 90 mA. For N14T, the crystals were briefly soaked in a solution containing 16% PEG 4 K and 100 mM NaCl in 50 mM Tris (pH 8.0) and flash frozen in a stream of nitrogen (Oxford cryo-system) at 100 K. The crystals of N14G, N14A, and N14Q were grown in the presence of cryo protectant and directly flash frozen without any prior soaking. The details of data collection for the mutants are given in Table 1. The data were processed using the programs DENZO and SCALEPACK of HKL package (*16*).

Structure Determination and Refinement. Among the mutants, N14A and N14Q crystallized in space group $P6_1$-22, isomorphous to the wild-type protein, with one molecule in the asymmetric unit. N14G and N14T, on the other hand, crystallized in triclinic and orthorhombic ($P2_12_12$) space groups, respectively, with two molecules in the asymmetric unit. Molecular replacement searches for the mutants that crystallized in nonisomorphous space groups were carried out using AMoRe (CCP4) (*17*), where the coordinates of rWCI (pdb code: 1EYL; *13*) were used as search model. The mutant N14T produced a correlation coefficient of 68.2% and R-factor of 35.3%, while N14G produced a correlation coefficient of 63.2% and R-factor of 37.8% with two molecules in the asymmetric unit. N14A and N14Q produced R factors of 35.3 and 37.2%, respectively, after rigid body refinement in CNS (*18*). All the structures were refined by alternating cycles of refinement in CNS and model rebuilding using 'O' (*19*). Progressive inclusions of water molecules dropped the R-factors to 21.1% (R_{free} = 26.3%), 21.3% (25.2%), 20.1% (25.4%), and 21.9% (23.8%) for N14G, N14A, N14T, and N14Q, respectively. The refinement statistics are given in Table 1.

Assay of Chymotrypsin Inhibitory Activity Using the Synthetic Substrate N-Benzoyl L-Tyrosine Ethyl Ester (BTEE). The chymotrypsin inhibitory activity of wild-type WCI and its mutants were assayed by measuring the esterolytic activity of chymotrypsin in the presence of the inhibitors, using BTEE as substrate. The stock solution of chymotrypsin (Sigma) was prepared by dissolving it in 0.001 N HCl to a concentration of 100 nM. The stock solution of WCI and the mutants were of 100 nM in 0.08 M Tris, 0.01 M $CaCl_2$ (pH 7.8) and BTEE (Sigma) was of 100 mM in 50% (W/V) methanol. For the determination of the residual enzymatic activity, varying amounts (3−30 nM) of each inhibitor was preincubated with a fixed amount of chymotrypsin (50 nM)

Table 2: Distances of C_α Atoms of Reactive Site Loop Residues of Each Mutant from that of WCI and the Distances of C_α Atoms of Reactive Site Loop Residues from the C_α of 14 Residue

	62 (P4) C_α	63 (P3) C_α	64(P2) C_α	65 (P1) C_α	66 (P1′) C_α	67 (P2′) C_α	68 (P3′) C_α
Distances of C_α Atoms of Reactive Site Loop Residues of Each Mutant from that of WCI							
N14G (1)	0.61	1.25	1.95	3.16	1.92	0.49	0.42
N14G (2)	0.96	1.41	2.43	3.15	1.92	0.82	0.27
N14A	0.47	0.30	0.43	0.33	0.46	0.53	0.45
N14T (1)	0.53	1.07	1.28	2.93	2.28	1.56	0.62
N14T (2)	0.22	0.83	1.02	1.48	1.27	1.34	0.43
N14Q	0.73	1.0	0.7	0.8	1.4	1.3	1.3
Distances of C_α Atoms of Reactive Site Loop Residues from the C_α of 14 Residue (for WCI and Mutants)							
WCI	6.3	9.4	8.5	8.0	6.8	5.3	4.8
N14G (1)	6.9	9.8	9.4	6.3	5.9	5.2	4.8
N14G (2)	7.0	10.1	9.5	6.1	5.8	4.6	5.3
N14A	6.6	9.9	9.0	8.1	7.1	5.3	5.0
N14T (1)	7.2	10.9	10.8	8.5	7.3	5.7	6.5
N14T (2)	7.0	10.4	10.32	8.6	7.4	5.4	6.2
N14Q	6.7	9.6	8.5	8.2	6.4	5.4	4.4

at 25 °C in a buffer containing 0.08 M Tris (pH 7.8) and 0.01 M $CaCl_2$. After the sample was incubated for 15 min, the residual enzymatic activity was monitored by measuring the rate of product formation at A_{256} (*20*) for 2 min using 200 nM of BTEE as substrate. All experiments were done in triplicate.

Limited Proteolysis of the Mutant Inhibitors by Chymotrypsin. A limited proteolysis experiment of WCI, N14A, and N14Q in the presence of chymotrypsin was carried out at 25 °C for 6 h in a reaction mixture containing 3 mg/mL of inhibitor and 0.03 mg/mL of chymotrypsin in 0.08 M Tris (pH 7.8) containing 0.01M $CaCl_2$. The reaction was terminated by addition of 1 mM PMSF and an equal volume of 2× sample buffer consisting of 0.25 M Tris-HCl (pH 6.8), 20% glycerol, 0.005% bromophenol blue, 4% SDS, 10% 2-mercaptoethanol followed by immediate boiling. The chymotryptic cleavage products of the WCI, N14A, and N14Q were analyzed by 15% SDS−PAGE stained by Coomasie R-250.

Database Analysis of Serine Protease Inhibitors. The crystal structure coordinates of the serine protease inhibitors of different families, either in the free state or in the complexed state with enzyme, were retrieved from structural database of PDB (http://www.rcsb.org), and their reactive site loop regions were analyzed in the graphical display of InsightII to identify the inhibitors possessing spacer Asn that interact with the reactive site loop. In case of a multiple entry of the same protein in PDB, only one entry was taken for analysis. As further criteria, the coordinates of the mutant inhibitors and NMR structures were not considered to prepare the database. The coordinates of the serine protease inhibitors possessing spacer Asn were then superposed, based only on their P2 and P1′ carbonyl C and O atoms, using the program InsightII, and the orientations of the side chain polar atoms of spacer Asn, relative to the reactive site loops, are compared for different inhibitors. Figures 1, 2, and 5 are prepared by MOLSCRIPT (*21*) and RASTER3D (*22*).

RESULTS

Overall Structural Comparison of the Mutants with WCI. All the mutant structures were well refined, and the accuracy of the refined models is consistent with the quality of the diffraction data. The $2F_o - F_c$ map for the entire polypeptide chain, in each case, is well developed, except for the residues of the N-terminus, C-terminus, and the flexible loop (His137−Lys143). Unambiguous electron densities are obtained for the reactive site loops and for the residues at the site of mutation. Since the mutants were crystallized in different space groups having different crystal packing and in some cases (N14G, N14T) with multiple molecules in the asymmetric unit, we have checked whether the structural changes, observed at the reactive site loop of the mutants, especially for N14T and N14G (as these crystals are not isomorphous to WCI crystals), are due to the mutation at the neighboring scaffold or if it is a crystal packing artifact. Our analysis, particularly considering the differences in contact with the symmetry-related molecules in different crystal forms, suggests that the reactive site loops of N14T and N14G are loosely packed, and their resulting conformation should not be influenced by crystal packing. Nonetheless, to avoid the effect of other loops involved in crystal packing, superpositioning for the structural comparison is done considering only the main chain atoms of the twelve β strands. According to this scheme, the superposition of N14T, N14G, N14A, and N14Q on WCI produce rmsd values of 0.46 (0.42), 0.38 (0.42), 0.23, and 0.24 Å, respectively (the value within parentheses is for the second molecule of the asymmetric unit). After superposition, the distances (C_α) of the reactive site loop residues (P4−P3′) of the mutants from the corresponding atoms of WCI were measured, which could provide the extent of loop deformation upon mutation at the 14th position, compared to the wild-type protein (Table 2). The $C_\alpha - C_\alpha$ distances of the loop residues (P4−P3′) from that of the 14th residue were also measured in individual cases, and the values are compared with that of WCI (Table 2).

Deformation of the Reactive Site Loop Region in N14T: The Effect of β-Branching at the 14th Position. At the mutation site, N14T experiences severe structural deformation: Thr14 shifts toward the core of the protein, which subsequently causes the repositioning of two consecutive glycines, Gly15 and Gly16—a feature that is observed for both molecules of N14T of the asymmetric unit. In WCI, the Glu13-Asn14-Gly15-Gly16 (X−N−G−G) motif forms a type-II β-turn with a hydrogen bond between Glu13 O and Gly16 N ($O_i - N_{i+3}$), where Gly15 and Gly16 are involved in a 'G1' β bulge with Ile60 at the tip of β4 (Figure 1b). The structural information on Kunitz (STI) type inhibitors indicate that these turn and bulge interactions are conserved

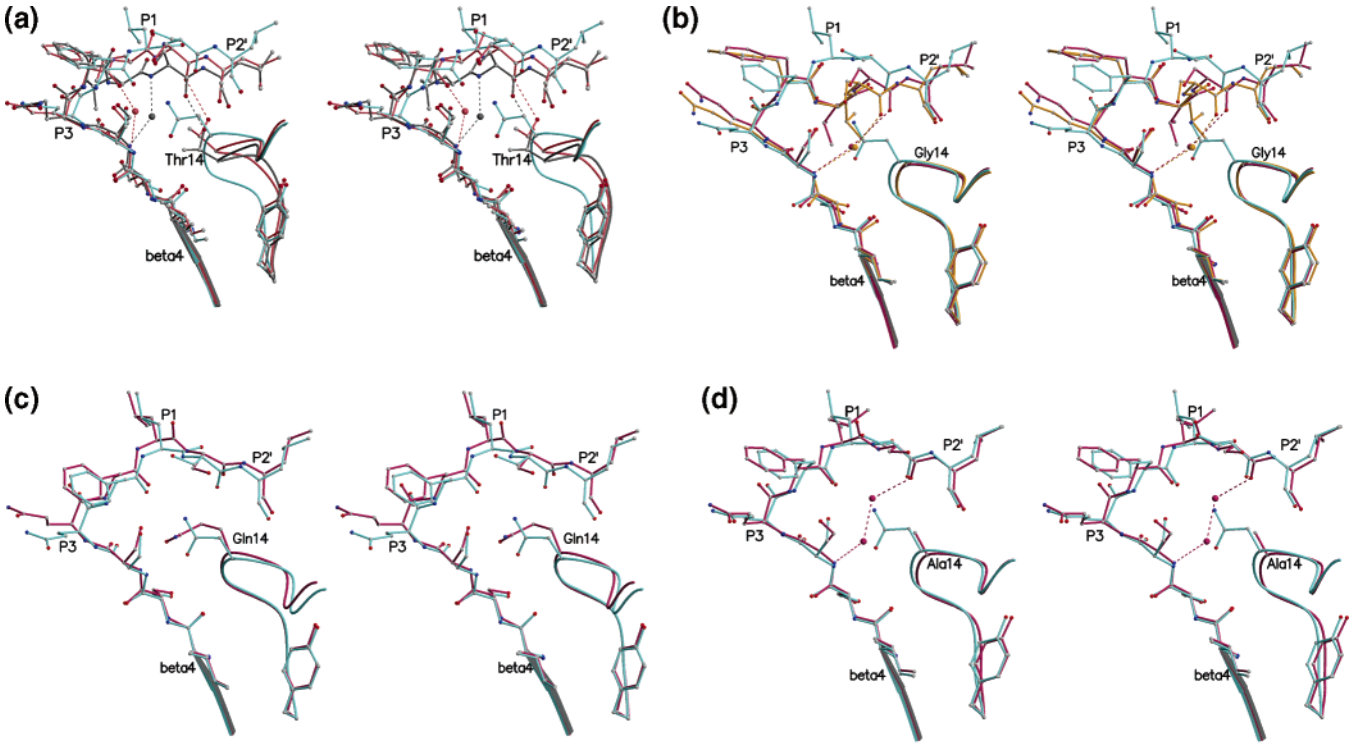

FIGURE 2: Stereoscopic representation of the structural changes at the reactive site loop and mutation site of (a) N14T-1 (moss) and N14T-2 (salmon pink) compared to that of WCI (sky blue). Water molecules of N14T are shown as balls and hydrogen bonds are shown as dotted lines. (b) N14G-1 (violet) and N14G-2 (yellow) compared to that of WCI (sky blue). Water molecules of N14G are shown as balls, and hydrogen bonds are shown as dotted lines. Conformational similarity between the reactive sites of (c) N14Q (violet) and WCI (sky blue) and (d) N14A (violet) with WCI (sky blue) are also shown here. Superposition for the comparison was made considering only the main chain atoms of 12 β-strands.

Table 3: ϕ/ψ Angles (°) for WCI and Mutants around the Reactive Site (P3−P3′)

	P3 (ϕ/φ)	P2 (ϕ/φ)	P1 (ϕ/φ)	P1′ (ϕ/φ)	P2′ (ϕ/φ)	P3′ (ϕ/φ)
WCI	−71/−18	−98/168	−82/−9	−55/158	−74/−29	−120/−174
N14G1	−62/−44	−91/16	42/40	−79/152	−35/−50	−124/−177
N14G2	−63/−33	−124/33	43/48	−69/129	−42/−49	−116/141
N14A	−78/−16	−110/153	−85/119	−168/162	−80/−20	−121/−171
N14T-1	−62/−12	−99/9	38/55	−126/179	−69/−45	−110/165
N14T-2	−40/−49	−96/154	−91/79	−122/170	−78/−55	−85/164
N14Q	−78/6	−110/149	−83/102	−155/161	−78/−28	−131/160

in this family. Superpositioning of N14T on WCI shows that C_α atom of Thr14 is moved toward the core by 2.23 (1.97) Å from the corresponding atom of WCI. This distortion is propagated to the other residues following Thr14 and merges at around Tyr18, so that the hydrogen bond between Tyr18 OH and Glu13 N is retained (Figure 2a). Because of the paucity of space, the residues between Glu13 and Tyr18 have no other option but to move away from β4 [the C_α atoms of Gly15 and Gly16 had been shifted by 3.7 (3.2) and 2.0 (1.8) Å from the corresponding atoms of WCI], destroying the β bulge interaction with Ile60 and the β turn interaction Glu13 O···Gly16 N (O_i−N_{i+3}) present in the wild-type protein (Figure 1). From Figure 1, it is further evident that in case of WCI, the C_β atom of Asn14 is within van der Waals distance of P1′ carbonyl O. The β-branched residue at the 14th position of N14T therefore creates a short contact with P1′, which is avoided in this case through the movement of the mutated site toward the core of the protein (Figure 2a). This huge structural rearrangement at the mutated site has an impact on the reactive site loop conformation, the extent of which is directly correlated with the movement of Thr14 toward the core: in N14T-1 the movement is greater, and the deviation is larger, whereas both are smaller in N14T-2 (Table 3). This difference does not disappear even when a local (P3−P3′) backbone superposition is done. N14T-2 superposes on WCI with an rmsd of 0.6 Å, whereas it is ∼1 Å for N14T-1 with maximum value at P1 of 1.2 Å. Nevertheless, the conserved main chain interaction between P2′ carbonyl O and the main chain N of the 14th residue is well restored in both the molecules. Thr14 adopts a χ1 angle of 47° (61° for N14T-2) such that in its present conformation, the OG atom forms a hydrogen bond with the P1′ carbonyl O. Interestingly, the newly created vacant space between Thr14 and the residues at the N-terminal part of the scissile bond (as evident in Table 2) is now occupied by a delocalized water molecule, which forms hydrogen bonds with P4 N and P1′ N in N14T-1 (moss-colored in Figure 2a) and P4 N and P2 O in N14T-2 (salmon pink in Figure 2a). All these facts mentioned above indicate that N14T molecules can exist in two different conformations, which have been trapped in the crystal lattice.

N14G Reactive Site: Loss of Canonical Conformation. The truncation of the Asn14 side chain to a hydrogen atom in N14G not only creates a vacant space in the concave side of the reactive site loop but also causes a loss of the hydrogen-bonding interactions made by the Asn14 side chain in WCI. Comparison with WCI shows that the reactive site loop of N14G experiences severe deformation (Figure 2b), and the values of the dihedral angles of the reactive site residues (Table 3) indicate that, unlike N14T, the extent of deformation is not very different in the two N14G molecules of the asymmetric unit. The backbone of the primary recognition residue Leu65 (P1) adopts a noncanonical conformation (with a ϕ/ψ values of 42/40 in N14G-1 and 43/48 in N14G-2, compared to −82/-9 of WCI), in such a way that the P1 residue, along with the scissile peptide bond, is now flipped toward the vacant space created by Asn → Gly mutation (Figure 2b). The solvent accessible surface area (*23*) of Leu65 (P1) side chain, calculated using a probe radius of 1.4 Å, is around 79% in N14G, in contrast to 100% accessibility for the wild-type protein WCI. A flipping of the P2−P1 peptide bond occurs (Table 3), where the P2 carbonyl O that was facing the ND2 atom of Asn14 in WCI, moves outward in N14G and faces the solvent. One water molecule is found near the reactive site loop of N14G, which is located corresponding to a position between the two polar atoms of Asn14 side chain (Figure 2b) and forms hydrogen bonds with P1′O and P4 N. Nonetheless, the $C_\alpha-C_\alpha$ distances between Gly14 and the residues of the reactive site loop subsite are consistently smaller in the case of N14G (Table 2). Calculation of the reactive site loop deformation for N14G (Table 2) shows a maximum value for P1 C_α (3.16 Å) followed by P2 C_α (2.43 and 1.92 Å) and P1′ C_α (1.92 Å) compared to WCI. Since the C_α atom of Gly14 is not displaced compared to WCI, the structural changes occurred for N14G point toward a reactive site loop conformation with less protrusion.

Retention of the Canonical Conformation of the Binding Loop by a Bigger Spacer in N14Q and a Smaller Spacer in N14A. The canonical conformation of the reactive site loop of N14Q is restored except the reorientation of P1 carbonyl O, as evident from the values of the dihedral angles (Table 3) and the local superposition (C_α) of P3−P3′ region (rmsd of 0.25 Å). Superposition of the 12 beta-stranded core of N14Q on that of WCI reveals a slight protrusion of the N14Q reactive site loop, which is noticeable at the C-terminal part of the scissile peptide bond (Table 2). The C_α atom of Gln14 is displaced here by 0.9 Å from the corresponding atom of WCI in such a way that the distances of the C_α atoms of the loop residues from that of Gln14 remain similar to that of WCI (Table 2). It is interesting to see how the longer side chain of Gln14 is oriented to retain the loop conformation. In WCI, all the side chain atoms of Asn14 and the C_α atoms of loop residues stay more or less in a plane. But it is difficult for the Gln14 side chain to be accommodated in the loop cavity like it is in WCI, which has been relieved by the movement of the C_β and C_γ atoms of Gln14 away from the loop compared to the corresponding atoms of Asn14. The side chain of Gln14 finally takes an unusual rotameric value of −145° at $\chi 3$ such that it places only the NE2 atom in the plane of the loop to interact with P4 Ser OG and P2 carbonyl O, while its OE1 atom stays away from the loop (Figure 2c). Although the side chain of Gln14 in this orientation helps the reactive site loop to maintain its protruded conformation, the NE2 atom is not in a position to simultaneously interact with P2 and P1′ carbonyl O (like the ND2 atom of Asn14) in the intact form of this mutant (Figure 2c).

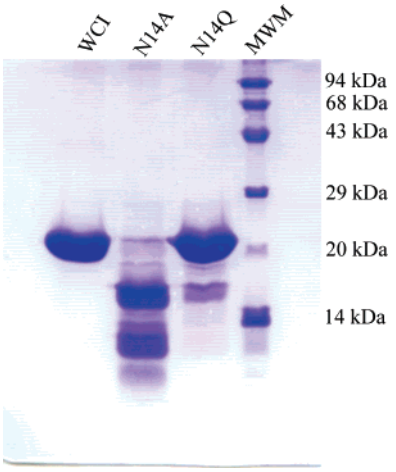

FIGURE 3: 15% SDS−PAGE showing the proteolysis products of WCI, N14A, and N14Q by chymotrypsin in 100:1 mixtures of inhibitor and enzyme, incubated for 6 h at 25 °C.

Aside from the flipping of P1 carbonyl O, the reactive site loop conformation of N14A is similar to that of WCI, as evident from the numerical values given in Tables 2 and 3 and from the pictorial representation of Figure 2d. The C_α atoms (P3−P2′) of N14A superposes on WCI with an rmsd value of 0.3 Å. Two water molecules were found in the vicinity of the reactive site forming hydrogen bonds with the loop residues: W1 forms a hydrogen bond with the carbonyl O of Phe64 (P2) and Ser66 (P1′), whereas W2 is hydrogen bonded with W1 and the N atom of Ser62 (P4). W1 and W2 are 3.7 and 3.83 Å away from Ala14 C_β atom, respectively, which is marginally beyond van der Waals distance. When superposed on WCI, the mutation site of N14A showed a movement of 0.7 Å toward the protein core (Figure 2d).

Limited Proteolysis of Inhibitors by Chymotrypsin. Structural results prompted us to compare the behavior of N14Q and N14A with WCI, in the presence of chymotrypsin, as both of these mutants possess the canonical binding loop conformation and are expected to behave as good inhibitors. Limited proteolysis of WCI, N14Q, and N14A with chymotrypsin was performed in an inhibitor/enzyme ratio of 100:1 (w/w), and, as expected, no cleavage product was seen for WCI. Nominal cleavage was seen for N14Q, but in contrast to our expectations N14A cleaved almost like a substrate (Figure 3).

Residual Enzymetic Activity of Chymotrypsin, in the Presence of the Mutants. To measure the inhibition of the esterolytic activity of chymotrypsin by WCI and its mutants, the residual activity of chymotrypsin (%), measured after enzyme inhibitor incubation of 15 min, was plotted against the inhibitor concentration (Figure 4). Results of residual activity measurements demonstrate that N14G is the weakest inhibitor, followed by N14L and N14T, while N14Q is the strongest among the mutants studied here (Figure 4). Surprisingly, N14A cannot inhibit chymotrypsin as much as expected from the observed canonical structure of its reactive site loop. The stoichiometry of inhibition was calculated by extrapolating the linear part of the curve to 0% residual

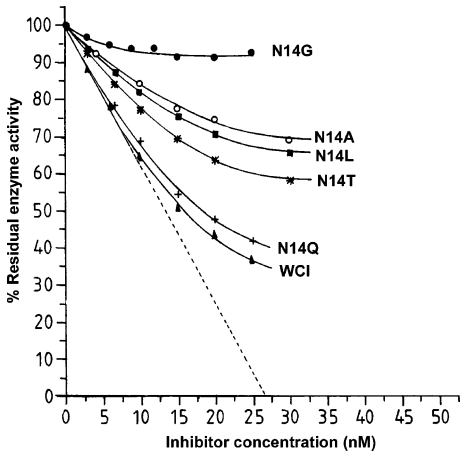

FIGURE 4: Inhibition of estarolytic activity of chymotrypsin by WCI and its mutants were measured. Chymotrypsin (50 nM) was incubated at 25 °C for (a) 3 min and (b) 15 min with varying amounts (2−30 nM) of inhibitors and assayed for the residual enzyme activity at A_{256}, taking 200 nM BTEE as substrate.

activity, which shows that WCI inhibits chymotrypsin in a 1:2 molar ratio (Figure 4), as reported by Kortt (*24*). The dissociation constant (K_i) for WCI, determined from the residual plot as described by Beith (*25*) is 1.93×10^{-9} M. The mutant N14Q inhibits chymotrypsin in a molar ratio close to 1:2, which is similar to WCI with a K_i value of 3.1×10^{-9} M. Since the residual enzyme activity profile does not show any inhibition of chymotrypsin by N14G and limited proteolysis experiments represent N14A like a substrate (Figure 3), we did not calculate the K_i values for these two mutants. However, the dissociation constants for N14T and N14L calculated as above are 7.06×10^{-8} M and 1.07×10^{-7} M respectively, which are lower than that of WCI by order of magnitude.

DISCUSSION

A number of mutations on Asn14 of WCI were made to critically investigate the role of this scaffolding residue in maintaining the reactive site loop conformation and its inhibitory function. The mutations were chosen with the intention to understand the effect of the residue size (Asn → Gln, residues of same electrostatic nature), electrostatic nature (Asn → Leu, residues of similar size), and both size and electrostatic nature (Asn → Thr, Asn → Ala and Asn → Gly) at the 14th position. The diversity of structural changes, in response to these mutations, range from subtle to substantial as seen in Table 2. The reactive site loop that was previously found in a single conformation in the native protein occupies multiple conformations in some mutants (N14G, N14T), indicating that the loop can acquire a flexible nature for them. Moreover, solvent molecules spatially replace the truncated side chain atoms, and they help to maintain the canonical conformation, in the case of N14A, while in N14G and N14T they fail to do so.

Structure analyses indicate that N14G should functionally be the least active among the mutant inhibitors studied, as its primary recognition residue (Leu65) is not as exposed as it should be for enzyme recognition, compared to other canonical inhibitors. The Asn → Gly mutation creates a cavity inside the loop, and the P1 recognition residue is found to flip toward that cavity. Three factors—loss of canonical conformation of the reactive site loop, its reduced protrusion, and loss of hyper solvent accessibility of P1 side chain (caused by the flip)—probably affect the inhibitory potency of N14G, as these factors are going against enzyme−inhibitor recognition. The reactive site loop conformation of the two molecules of N14T are distinctly different from each other as N14T-2 is not very different from WCI, while N14T-1 resembles N14G more with its reactive site showing less protrusion. From the sequence analysis of the Kunitz (STI) family inhibitors, we noticed a conserved 'X−N−G−G' motif (where N corresponds to the conserved Asn), and structural analyses of WCI, ETI, and STI showed that this motif forms a type-II β turn, which is strategically located to project the side chain of Asn14 into the reactive site loop cavity. Loss of these important β-turn and β-bulge interactions, in the case of N14T, generates flexibility at this region and is reflected in the variable deformation of the reactive site loop.

With the observed noncanonical structures of the binding loop, one cannot expect that N14G and N14T (molecule type N14T-1) would follow the standard mechanism of protease inhibition. Residual enzyme activity experiments (Figure 4) present N14G as the weakest inhibitor, which is in accordance with the structural observations. The residual activity of N14T falls between WCI and N14G. Considering that the N14T molecule stays in two conformations in solution, as trapped in a crystal lattice, N14T-1 should behave like N14G, while N14T-2 is expected to behave somewhat like WCI as far as inhibition is concerned. Modeling the reactive site loop of the mutants in the active site groove of chymotrypsin, considering STI−PPT complex as template (PDB code: 1AVW; *6*), also showed that the P1 recognition residue of N14G (both the molecules) and N14T-1 cannot be fitted in the S1 specificity pocket of chymotrypsin, and their P1 carbonyl O do not point toward the oxyanion hole. However, a minor conformational adjustment helps the reactive site of N14T-2 to fit in the active site groove of chymotrypsin. The inhibition profile observed in the case of N14T may therefore be the result of predominant binding of the molecule type N14T-2. The lesser inhibition of N14L, seen in the residual enzyme activity profile, can probably be attributed toward its reduced recognition due to the loss of the canonical conformation of the binding loop, caused by the presence of the hydrophobic residue Leu at the 14th position, as predicted in our previous molecular dynamics studies (*14*).

The reactive site loop conformation of N14A and N14Q, on the other hand, are fairly similar to WCI, both at the backbone and side chain level. On the basis of this observation, it is expected that N14A and N14Q will be able to bind and inhibit the enzyme in a manner similar to WCI. However, the inhibitory behavior of N14A, as seen in the residual enzyme activity profile, is surprising. N14A fails to inhibit chymotrypsin, as evident in Figure 4, which is further supported by the limited proteolysis experiment (Figure 3) where proteolysis of N14A occurred almost completely. The lower inhibitory activity of N14A (Figure 4), despite having a canonical reactive site loop, can only be explained when the results of limited proteolysis experiments are considered. Figure 3 shows that N14A is hydrolyzed almost completely by chymotrypsin and therefore incapable of inhibiting the enzyme, a situation more like a substrate than an inhibitor.

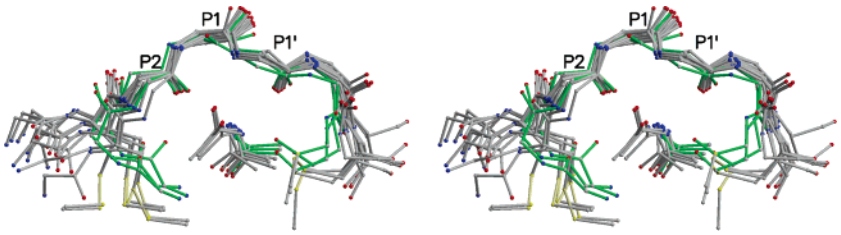

FIGURE 5: Superposition of the reactive site loops (P4−P3′) and spacer aspergines of fourteen inhibitors, belonging to different families of serine protease inhibitors are represented stereoscopically. The inhibitors of Kunitz (STI) family, i.e., 1EYL, 1TIE and 1AVW are shown in different stick color (green) from the rest of the inhibitors.

Table 4: Families of Serine Protease Inhibitors Possessing Spacer Asn

family name/ MEROP ID (34)	coordinates taken	P1−P1′	Asn position	nearest preceding Cys from P1	nearest following Cys from P1	ref
Kunitz (STI)/I3	1EYL	65−66	14	P25	P23′	13
	1TIE	63−64	12			10
	1AVW	63−64	13			6
Kazal/I1	2OVO	18−19	33	P3	P6′	26
	1HPT	18−19	33			27
	1YU6	18−19	33			28
	1TBR	10−11	25			29
ecotin/I11	1IFG	84−85	51	P35	P3′	30
SSI/I16	2SIC	73−74	99	P3	P28′	31
grasshopper/I19	1GL1	30−31	15	P3	P3′	32
	1YR4	29−30	15			33
potato II/I20	4SGB	38−39	5	P3	P2′	34
	1PJU	62−63	29			35

In contrast to N14A, the residual enzyme activity in the presence of N14Q is quite close to that of WCI (Figure 4), which is in agreement with the nominal cleavage product for N14Q seen in the limited proteolysis experiments (Figure 3).

A good inhibitor should retain the amide group, formed after the cleavage of the scissile peptide bond, in a place suitable for religation, which can ease the formation of the thermodynamically favorable Micelle complex rather than the acyl enzyme intermediate (*3*). Our study reveals the nature of a residue at the crucial scaffolding position, optimized in size and charge, required for a good inhibitor, especially for the Kunitz (STI) family. We see that the methyl group of Ala14 and two water molecules together are capable of maintaining the canonical conformation of the binding loop of N14A for proper enzyme recognition, but they are not suitable enough to captivate the cleaved parts together for religation, and this in turn renders N14A vulnerable to proteolysis (Figure 3). The nature of this amino acid residue seems to be crucial for a spacer bigger than Ala, as we see that a β-branched residue distorts the loop structure in N14T, whereas a spacer of almost the same size as Asn i.e., Leu makes N14L a poor inhibitor. Comparison of N14L and WCI demonstrate that although the size of their spacer is same the difference in their chemical nature creates a significant alteration in their inhibitory property. In WCI, the side chain ND2 atom of Asn14 forms two hydrogen bonds with P2 and P1′ carbonyl O at either side of the scissile bond, which presumably holds the cleavage products together for religation and keeps the turnover following acylation remarkably slow, making WCI a potent inhibitor. In N14Q, although the polar terminal NE2 atom of Gln14 is incapable of forming hydrogen bonds with P2 and P1′ carbonyl O simultaneously in the intact inhibitor, a slight reorientation of the Gln14 side chain may occur after the cleavage of the scissile peptide bond, allowing the NE2 atom to arrest the two fragments together for religation. However, the small loss of the inhibitory potency of N14Q can be attributed to the strained accommodation of the Gln14 side chain, having one extra methyl group, compared to Asn. Considering the canonical binding of the inhibitor to the enzyme, cleavage of the scissile peptide bond and subsequent religation (k_{-2}), the scaffolding residue Asn14 appears to be the most suitable, as it snugly fits into the concave space of the reactive site loop cavity and its chemical compatibility allows ND2 atom to flank the cleavage site, favoring religation without any conformational rearrangement or strain relief, both in intact and cleaved inhibitor.

Role of Asn Residue as a Spacer in Serine Protease Inhibitors: A Database Analysis. To survey the protein scaffold−binding loop interactions in serine protease inhibitors other than Kunitz (STI), we have performed a structural database analysis. Out of 18 convergently evolved families of serine protease inhibitors, crystal structures are available for 12 families. Our database analysis reveals that out of these, the inhibitors of six families (Table 4) possess a spacer Asn, which is highly conserved within the respective family. It is however to be noted that aside from the Kunitz (STI) family, five other families have the reactive site loop connected to the protein scaffold by disulfide bridges (mostly at P3) in addition to the spacer Asn. The inhibitors, listed in Table 4, widely differ in their size (ranging from 30 to 200 amino acids, approximately), sequence, overall folding and disulfide bridge pattern (*36*). However, when the inhibitory loops of these inhibitors were superposed, based only on their P2 and P1′ carbonyl groups, we see that although the side chain of Asn of different inhibitors approaches from different directions, the ND2 atoms of these Asn residues cluster tightly at a particular position so that it can form hydrogen bonds with P2 and P1′ carbonyl O (Figure 5). The conserved

nature of these Asn residues, their space availability and strikingly similar disposition of their ND2 atoms around scissile bond (as in WCI) lead us to speculate that in all these five families of inhibitors the spacer Asn plays a similar role in the religation mechanism.

It is a well-known fact that the inhibitory loop of serine protease inhibitors possesses a protruding shape with a characteristic canonical conformation (*2*, *3*). But the important feature we noted was that this conformation, while keeping the P1 side chain hyper solvent accessible, leaves the carbonyl O atoms of P2 and P1′ residues projecting toward the concave side of the loop. Hence, after acyl-enzyme formation, the process of reconstruction of the scissile peptide bond will definitely be facilitated by the presence of an amino acid in the vicinity having a hydrogen-bond donor atom which is able to clamp the P2 and P1′ carbonyl oxygens. The reactive site loop of the inhibitors, belonging to the Kunitz (STI) family, differs from others in terms of their characteristic narrow curvature where it houses only a spacer Asn in the absence of any disulfide bridge nearby. In Figure 5, we see that in the case of the inhibitors having wide reactive site loop curvature, disulfide bridges (either at P3 or P3′) reduce that curvature effectively to that of Kunitz (STI) inhibitors. Although these disulfide bridges play a major role in stabilizing the reactive site loop conformation, they are probably inadequate to hold the cleaved parts together for religation, which is accomplished by the ND2 atom of the spacer Asn. A network of hydrogen bonds involving a number of loop residues and parallel spacer arginines is observed in CI-2 of the PI-1 family, which is required to provide stability to the reactive site loop, as the reactive site loop of this inhibitor is wide and is devoid of any support from disulfide bridges (*3*). But in this inhibitor also, the hydrogen-bond donor atom for religation is contributed only by the two spacer arginines (*7*). However, the Asn-mediated religation process seems to be prevalent in serine protease inhibitors, as spacer Asn can dispose its ND2 atom as a hydrogen-bond donor for both P2 and P1′ carbonyl oxygen atoms. These observations as a whole help in differentiating the common chemical requirement of religation from the diverse stability requirement of the reactive site loop which varies for different inhibitors depending on their loop curvature and presence of disulfide bridges in the vicinity of the reactive site.

ACKNOWLEDGMENT

J.D. thanks Sophia Tsai of MCB, USC, for her valuable assistance in checking the language of the revised manuscript.

NOTE ADDED AFTER ASAP PUBLICATION

An earlier version of this paper posted ASAP on the Web on May 17, 2006, did not include a description or a link to Supporting Information. This has been added in this new version posted May 18, 2006.

SUPPORTING INFORMATION AVAILABLE

Stereoscopic presentation (Figure S1) of the reactive site loop along with the mutation site for (a) N14T, (b) N14G, (c) N14Q, and (d) N14A. This material is available free of charge via the Internet at http://pubs.acs.org.

REFERENCES

1. Laskowski, M., Jr., and Kato, I. (1980) Protein inhibitors of proteinases, *Annu. Rev. Biochem. 49*, 593−626.
2. Bode, W., and Huber, R. (1992) Natural protein proteinase inhibitors and their interaction with proteinases, *Eur. J. Biochem. 204*, 433−451.
3. Radisky, E. S., and Koshland, D. E., Jr. (2002) A clogged gutter mechanism for protease inhibitors, *Proc. Natl. Acad. Sci. U.S.A. 99*, 10316−10321.
4. Laskowski, M., Jr., and Qasim, M. A. (2000) What can the structures of enzyme−inhibitor complexes tell us about the structures of enzyme substrate complexes? *Biochem. Biophys. Acta 1477*, 324−337.
5. Dattagupta, J. K., Podder, A., Chakrabarti, C., Sen, U., Dutta, S. K., and Singh, M. (1996) Structure of a Kunitz-type chymotrypsin from winged bean seeds at 2.95 Å resolution, *Acta Crystallogr. D52*, 521−528.
6. Song, H., K., and Suh, S., W. (1998) Kunitz-type soybean trypsin inhibitor revisited: refined structure of its complex with porcine trypsin reveals an insight into the interaction between a homologous inhibitor from *Erythrina caffra* and tissue-type plasminogen activator, *J. Mol. Biol. 275*, 347−363.
7. Radisky, E. S., Lu, C. J., Kwan, G., and Koshland, D. E., Jr. (2005) Role of the intramolecular hydrogen bond network in the inhibitory power of chymotrypsin inhibitor 2, *Biochemistry 44*, 6823−6830.
8. Radisky, E. S., King, D. S., Kwan, G., and Koshland, D. E., Jr. (2003) The role of the protein core in the inhibitory power of the classic serine protease inhibitor, chymotrypsin inhibitor 2, *Biochemistry 42*, 6484−6492.
9. Radisky, E. S., Kwa, G., Karen, Lu, C. J., and Koshland, D. E., Jr. (2004) Binding, proteolytic, and crystallographic analyses of mutations at the protease-inhibitor interface of the subtilisin BPN′/chymotrypsin inhibitor 2 complex, *Biochemistry 43*, 13648−13656.
10. Onesti, S., Brick, P., and Blow, D. M. (1991) Crystal structure of a Kunitz-type trypsin inhibitor from Erythrina caffra seeds, *J. Mol. Biol. 217*, 153−176.
11. Meester, P. De, Brick, P., Lloyd, L. F., Blow, M. D., and Onesti, S. (1998) Structure of the Kunitz-type soybean trypsin inhibitor (STI): implication for the interactions between members of the STI family and tissue-plasminogen activator, *Acta Crystallogr. D54*, 589−597.
12. Dattagupta, J. K., Podder, A., Chakrabarti, C., Sen, U., Mukhopadhyay, D., Dutta, S. K., and Singh, M. (1999) Refined crystal structure (2.3 Å of a double-headed winged bean alpha-chymotrypsin inhibitor and location of its second reactive site, *Proteins: Struct. Funct., Genet. 35*, 321−331.
13. Ravichandran, S., Dasgupta, J., Chakrabarti, C., Ghosh, S., Singh, M., and Dattagupta, J., K. (2001) The role of Asn14 in the stability and conformation of the reactive-site loop of winged bean chymotrypsin inhibitor: crystal structures of two point mutants Asn14 → Lys and Asn14 → Asp, *Protein Eng. 14*, 349−357.
14. Dasgupta, J., Sen, U., and Dattagupta, J. K. (2003) In silico mutations and molecular dynamics studies on a winged bean chymotrypsin inhibitor protein, *Protein Eng. 16*, 489−496.
15. Khamrui, S., Dasgupta, J., Dattagupta, J. K., and Sen, U. (2005) Single mutation at P1 of a chymotrypsin inhibitor changes it to a trypsin inhibitor: X-ray structural (2.15 Å) and biochemical basis, *Biochim. Biophys. Acta 1752*, 65−72.
16. Otwinowski, Z., and Minor, W. (1997) Processing of X-ray diffraction data collected in oscillation mode, *Methods Enzymol. 276*, 307−326.
17. Collaborative Computational Project, Number 4 (1994) The CCP4 suite: programs for protein crystallography, *Acta Crystallogr. D50*, 760−763.
18. Brünger, A. T., Adams, P. D., Clore, G. M., DeLano, W. L., Gros, P., Grosse-Kunstleve, R. W., Jiang, J.-S., Kuszewski, J., Nilges, M., Pannu, N. S., Read, R. J., Rice, L. M., Simonson, T., and Warren, G. L. (1998) Crystallography & NMR system: A new software suite for macromolecular structure determination, *Acta Crystallogr. D54*, 905−921.
19. Jones, T. A., Zou, J. Y., Cowan, S. W., and Kjeldgaard, M. (1991) Improved methods for building protein models in electron density maps and the location of errors in these models, *Acta Crystallogr. A47*, 110−119.
20. Walsh, K. A., and Wilcox, P. E. (1970) Serine proteases, *Methods Enzymol. 19*, 31−41.

21. Kraulis, P. J. (1991) MOLSCRIPT: A program to produce both detailed and schematic plots of protein structures, *J. Appl. Crystallogr*. *24*, 946−950.
22. Merritt, E. A., and Bacon, D. J. (1997) Raster3D: Photorealistic Molecular Graphics, *Methods Enzymol*. *277*, 505−524.
23. Fraczkiewicz, R., and Braun, W. (1998) Exact and efficient analytical calculation of the accessible surface areas and their gradients for macromolecules, *J. Comput. Chem. 19*, 319−333.
24. Kortt, A. A. (1980) Isolation and properties of a chymotrypsin inhibitor from winged bean seed (*Psophocarpus tetragonolobus* (L) Dc.), *Biochim. Biophys. Acta 624*, 237−248.
25. Bieth, J. G. (1995) Theoretical and practical aspects of proteinase inhibition kinetics, *Methods Enzymol. 248*, 59−84.
26. Bode, W., Epp, O., Huber, R, Laskowski, M., Jr., and Ardelt, W. (1985) The crystal and molecular structure of the third domain of silver pheasant ovomucoid (OMSVP3), *Eur. J. Biochem. 147*, 387−395.
27. Hecht, H. J., Szardenings, M., Collins, J., and Schomburg, D. (1992) Three-dimensional structure of a recombinant variant of human pancreatic secretory trypsin inhibitor (Kazal type), *J. Mol. Biol*. *225*, 1095−1103.
28. Maynes, J. T., Cherney, M. M., Qasim, M. A., Laskowski, M., Jr., and James, M. N. G. (2005) Structure of the subtilisin Carlsberg-OMTKY3 complex reveals two different ovomucoid conformations, *Acta Crystallogr. D-Biol. Crystallogr. 61*, 580−588.
29. van de Locht, A., Lamba, D., Bauer, M., Huber, R., Friedrich, T., Kroger, B., Hoffken, W., and Bode, W. (1995) Two heads are better than one: crystal structure of the insect derived double domain Kazal inhibitor rhodniin in complex with thrombin, *EMBO J. 14*, 5149−5157.
30. Eggers, C. T., Wang, S. X., Fletterick, R. J., and Craik, C. S. (2001) The role of ecotin dimerization in protease inhibition, *J. Mol. Biol*. *308*, 975−991.
31. Takeuchi, Y., Satow, Y., Nakamura, K. T., and Mitsui, Y. (1991) Refined crystal structure of the complex of subtilisin BPN′ and *Streptomyces subtilisin* inhibitor at 1.8 Å resolution, *J. Mol. Biol*. *221*, 309−325.
32. Roussel, A., Mathieu, M., Dobbs, A., Luu, B., Cambillau, C., and Kellenberger, C. (2001) Complexation of two proteic insect inhibitors to the active site of chymotrypsin suggests decoupled roles for binding and selectivity, *J. Biol. Chem. 276*, 38893−38898.
33. Fodor, K., Harmat, V., Hetenyi, C., Kardos, J., Antal, J., Perczel, A., Patthy, A., Katona, G., and Graf, L. (2005) Extended intermolecular interactions in a serine protease-canonical inhibitor complex account for strong and highly specific inhibition, *J. Mol. Biol*. *350*, 151−169.
34. Greenblatt, H. M., Ryan, C. A., and James, M. N. (1989) Structure of the complex of *Streptomyces griseus* proteinase B and polypeptide chymotrypsin inhibitor-1 from Russet Burbank potato tubers at 2.1 Å resolution, *J. Mol. Biol. 205*, 201−228.
35. Barrette-Ng, I. H., Ng, K. K., Cherney, M. M., Pearce, G., Ghani, U., Ryan, C., A., and James, M. N. (2003) Unbound form of tomato inhibitor-II reveals interdomain flexibility and conformational variability in the reactive site loops, *J. Biol. Chem. 278*, 31391−31400.
36. Rawlings, N. D., Tolle, D. P., and Barrett, A. J. (2004) MEROPS: the peptidase database, *Nucleic Acids Res. 32*, D160−D164.

BI060374Q